Modeling Zinc in Biomolecules with the Self Consistent Charge-Density Functional Tight Binding (SCC-DFTB) Method: Applications to Structural and Energetic Analysis

MARCUS ELSTNER,[1,4] QIANG CUI,[2] PETRA MUNIH,[2] EFTHIMIOS KAXIRAS,[1]
THOMAS FRAUENHEIM,[4] MARTIN KARPLUS[2,3]

[1]*Department of Physics, Harvard University, Cambridge, Massachusetts 02138*
[2]*Department of Chemistry and Chemical Biology, Harvard University, Cambridge, Massachusetts 02138*
[3]*Laboratoire de Chimie Biophysique, ISIS, Universitè Louis Pasteur, 67000 Strasbourg, France*
[4]*Department of Theoretical Physics, University of Paderborn, D-33098 Paderborn, Germany*

Received 10 April 2002; Accepted 5 September 2002

Abstract: Parameters for the zinc ion have been developed in the self-consistent charge density functional tight-binding (SCC-DFTB) framework. The approach was tested against B3LYP calculations for a range of systems, including small molecules that contain the typical coordination environment of zinc in biological systems (cysteine, histidine, glutamic/aspartic acids, and water) and active site models for a number of enzymes such as alcohol dehydrogenase, carbonic anhydrase, and aminopeptidase. The SCC-DFTB approach reproduces structural and energetic properties rather reliably (e.g., total and relative ligand binding energies and deprotonation energies of ligands and barriers for zinc-assisted proton transfers), as compared with B3LYP/6-311+G** or MP2/6-311+G** calculations.

 J Comput Chem 24: 565–581, 2003

Key words: zinc; density functional tight binding; binding energy; deprotonation energy; proton transfer

Introduction

Zinc is an important element in both modern synthetic chemistry[1] and in living systems.[2] In synthetic chemistry, for example, zinc has been used to develop artificial catalysts for reactions such as selective phosphate hydrolysis.[3] In biological systems, zinc is the second-most abundant transition metal following iron. Despite the fact that it is redox inactive, the zinc ion plays versatile roles in proteins and protein-DNA complexes. One of these is maintaining structural stability;[4] examples include the zinc-finger class of transcriptional activation factors and retroviral proteins,[5,6] alcohol dehydrogenase (ADH),[7] and transcarbamoyltransferase.[8] Zinc ions that contribute to catalysis are found in more than 300 enzymes,[2] and the reactions catalyzed by zinc involve hydrolytic, condensation, and other atom and group transfer reactions. The reasons that zinc is often used for these reactions include its flexible coordination geometry, fast ligand exchange, Lewis acidity, intermediate polarizability (hard-soft character), availability, and strong binding to a suitable site.[9] For example, due to its +2 charge, zinc can shift the pK_a of weak acids, such as water, alcohol, and Cys sidechain, so as to generate deprotonated species that can act as strong nucleophiles in enzyme catalysis. Best known examples of zinc enzymes include carbonic anhydrase (CA),[10] ADH,[7] and carboxypeptidase.[11] The zinc charge has also been proposed as a modulator of the redox potentials of nearby metal ions, such as in the Zn, Cu-superoxide dismutase.[12] In certain systems, more than one zinc ion appears to be involved in either the catalysis (e.g., phospholipase,[13] alkaline phosphatase,[14] and amino peptidase[75]) or metal transfer (e.g., metallothioneins[15]).

To perform molecular dynamics or Monte Carlo simulations on biological systems containing zinc, empirical approaches have been proposed to describe the zinc-ligand interactions. Both bonded[16,17] and nonbonded[18,19] models have been proposed. It was demonstrated[19] that the nonbonded model can lead to an accurate and efficient description of the zinc-binding site in proteins, while

Correspondence to: M. Karplus

This article includes Supplementary Material available from the authors upon request or via the Internet at ftp://ftp.wiley.com/public/journals/jcc/suppmat/24/565 or http://www.interscience.wiley.com/jpages/0192-8651/suppmat/v24.565.html

allowing ligand exchange to occur.[20] More complicated forms of molecular mechanics (MM) potentials [e.g., the sum of interactions between fragments *ab initio* computed (SIBFA) model[21]] have been developed for zinc, and applications to small zinc-containing complexes have yielded promising results.[22] Such MM models cannot be used to investigate catalytic processes that involve bond breaking and formation in zinc-containing enzymes; for this purpose, quantum mechanical (QM) methods have to be applied. Although traditional *ab initio* or density functional theory calculations can give rather accurate structural and energetic results for systems containing zinc, the large computational expense involved has limited their use to small molecules[23] and molecular complexes, such as hydrated zinc ions[24] and model compounds for the zinc-protein interactions.[25] For the investigation of larger compounds, semiempirical methods like the standard AM1,[26] PM3,[27] and MNDO/d[28,29] models have been applied in various studies of zinc-containing systems. The performance of these models for structural and energetic properties of these systems has been investigated recently,[29] indicating several shortcomings and difficulties in the description of Zn complexes relevant to the biomolecular modeling. The introduction of QM/MM techniques in the last decade has made it possible to study enzymatic reactions at the quantum level without neglecting the effects of the protein environment. However, the size of the active sites of interest make QM/MM studies at the *ab initio* or density functional (DF) levels of theory still computationally very demanding. Given the importance of zinc-containing enzymes, a fast quantum method giving accurate structures and energetics is highly desirable.

A new approach, called the self-consistent-charge density functional tight binding (SCC-DFTB) method, has been developed recently.[30] It is based on a second-order expansion of the Kohn-Sham total energy with respect to charge density. In contrast to non–self-consistent tight-binding approaches,[31] this method introduces relaxation of the charge density at the level of Mulliken populations. Inclusion of the relaxation effect has greatly decreased the dependence of the results on the initial density and increased the transferability of parameters. The computational speed is determined by the solution of the generalized eigenvalue problem for the valence electrons, represented in a minimal basis of atomic-like orbitals. Therefore, it is comparable in the speed to the semiempirical MNDO, AM1, and PM3 methods, and two to three orders of magnitude faster than *ab initio* and DFT methods. All parameters of the SCC-DFTB model are calculated from DFT; no fitting to experimental data is involved. The method has been applied to calculate the energies, geometries, and vibrational frequencies of small organic molecules and peptides,[32,33,35] and the resulting mean average deviations from the experimental values were comparable to those of full DFT calculations with a double-zeta plus polarization basis set.[34] Good results were also obtained in applications to biologically relevant molecules, including structures of hydrogen-bonded complexes (e.g., HCOOH dimer, NH_4^+—NH_3), small peptides, and base pairing and stacking interactions.[35] The utility of the method has been extended recently by interfacing it with CHARMM[36] in a QM/MM framework,[37] and it has been demonstrated that the SCC-DFTB/MM approach is a promising way to explore the catalytic mechanisms of enzymes.[59]

In the present article, we describe the development of SCC-DFTB parameters for zinc and certain applications that illustrate their utility. The next section briefly reviews the SCC-DFTB approach and describes the parameterization procedure. In the section Test Calculations, we apply the new parameterization to a number of systems, including small complexes involving typical zinc ligands and active site models for a number of zinc-containing enzymes (CA, ADH, and amino peptidase).

Methods and Parameterization

SCC-DFTB Approach

Because detailed descriptions of the SCC-DFTB method have been given elsewhere,[30,37] we review it only briefly to define the notation and provide a framework for the description of the fitting procedure.

The method originated from density functional theory (DFT) through a second order expansion of the DFT total energy with respect to charge density variation, $\delta\rho$, relative to a chosen reference density, ρ_0. The total energy can be written as

$$E = \sum_i^{\text{occ}} \langle \phi_i | \hat{H}^0 | \phi_i \rangle + \frac{1}{2} \iint \left(\frac{1}{|\vec{r} - \vec{r}'|} + \left. \frac{\delta^2 E_{\text{xc}}}{\delta\rho\delta\rho'} \right|_{\rho_0} \right) \times \rho(\vec{r}) \delta\rho'(\vec{r}') d\vec{r} d\vec{r}' \left\{ - \frac{1}{2} \iint \frac{\rho_0'(\vec{r}')\rho_0(\vec{r})}{|\vec{r} - \vec{r}'|} d\vec{r} d\vec{r}' + E_{\text{xc}}[\rho_0(\vec{r})] - \int V_{\text{xc}}[\rho_0]\rho_0(\vec{r}) d\vec{r} + E_{\text{core}} \right. \quad (1)$$

where the ϕ_i are the Kohn-Sham orbitals and E_{xc} and V_{xc} represent the exchange-correlation energy functional and potential, respectively. The symbol $\hat{H}^0$ stands for the effective Kohn-Sham Hamiltonian, which depends only on the reference density, ρ_0:

$$\hat{H}_0 = -\frac{1}{2}\nabla^2 - \sum_k \frac{Z_k}{|\vec{R}_k - \vec{r}|} + \int \frac{\rho_0(r')}{|\vec{r} - \vec{r}'|} d\vec{r}' + V_{\text{xc}}[\rho_0(r)] \quad (2)$$

where Z_k is the charge of the kth nucleus. The second term in eq. (1) corresponds to the contribution of the density variations to the total energy; the third term within the braces represents the correction for the double counting of terms from the Coulombic and exchange-correlation contributions included in the $\hat{H}^0$ matrix elements; and the last term, E_{core}, is the effective core-core repulsion energy, which plays an important role in the parameterization (see below).

To obtain the SCC-DFTB energy expression, a number of approximations are introduced into eq. (1). As in most other semiempirical methods,[26,27,38] only the valence electrons are treated explicitly, and the Hamiltonian matrix elements $\langle \phi_i | \hat{H}^0 | \phi_i \rangle$ are represented in a *minimal basis* of localized pseudo-atomic Slater orbitals, χ_μ:

$$\phi_i = \sum_\mu c_\mu^i \chi_\mu \tag{3}$$

To determine χ_μ, the neutral atom valence electron DFT problem is solved with an additional harmonic potential, in the form of $(r/r_0)^2$, to localize the orbitals.[39] For the determination of the confinement radius, r_0, a variational principle could be applied in the framework of DFT[40]; for SCC-DFTB, a semiempirical approach is taken and trial calculations have shown that the choice $r_0 = (1.8 \approx 2.0)^* r_{\text{cov}}$ (where r_{cov} is the covalent radius of the element, as obtained from ref. [41]) is satisfactory. The Hamiltonian matrix elements in this linear combination of atomic orbital (LCAO) basis, $H^0_{\mu\nu} \equiv \langle \chi_\mu | \hat{H}^0 | \chi_\nu \rangle$, are then obtained as follows. The diagonal elements, $H^0_{\mu\mu}$, are taken to be the calculated atomic Kahn-Sham orbital eigenvalues, and the nondiagonal elements are calculated with a two-center approximation:

$$H^0_{\mu\nu} = \langle \chi_\mu | \hat{T} + V_{\text{eff}}[\rho_0^{\text{A}} + \rho_0^{\text{B}}] | \chi_\nu \rangle, \ \mu \in \text{A}, \ \nu \in \text{B} \tag{4}$$

where V_{eff} is the effective Kohn-Sham potential (Coulombic plus exchange-correlation) and ρ_0^{A} is the electron density of the *neutral* atom A; A and B define the two atoms. The Hamiltonian matrix elements, $H^0_{\mu\nu}$, and the overlap matrix elements, $S_{\mu\nu}$, are computed and tabulated with respect to the interatomic distances between A and B. The values of these matrix elements are obtained by interpolation of the tabulated data; this is one of the factors that makes the SCC-DFTB calculation fast.

The second order terms in the density variation, $\delta\rho$, relative to the reference density, ρ_0, are approximated by a superposition of atom-centered point charges:

$$\delta\rho = \sum_{\text{A}} \delta\rho^{\text{A}} \tag{5a}$$

$$\delta\rho^{\text{A}} \approx \Delta q^{\text{A}} = q^{\text{A}} - q_0^{\text{A}} \tag{5b}$$

The quantity q_0^A is equal to the number of valence electrons of the neutral atom A, and q^{A} is the population from a Mulliken analysis. The second derivative of the total energy with respect to the charge density fluctuations, $\partial^2 E / \delta\rho \delta\rho' |_{\rho_0}$, is approximated by a function γ_{AB}. In the limit A = B, the quantity $\gamma_{\text{AA}}/2$ is approximated[42] by the chemical hardness[43] of the atomic species, and is calculated with a large Slater basis set using Janacks theorem as the derivative of the energy of the highest occupied molecular orbital (HOMO) level with respect to its occupation number.[30] In the case of A≠B, a new functional form for γ_{AB} was proposed based on the analysis of Coulombic interaction between two exponentially decaying spherical charge distributions centered on the two nuclei (characterized with exponent τ_{A} and τ_{B}, respectively):[30]

$$\gamma_{\text{AB}} = \int\int \frac{s(\tau_{\text{A}}, R_{\text{A}}) s(\tau_{\text{B}}, R_{\text{B}})}{|r - r'|} dr dr' = \frac{1}{R_{\text{AB}}} - [e^{-\tau_{\text{A}} R_{\text{AB}}} K(\tau_{\text{A}}, \tau_{\text{B}}, R_{\text{AB}}) + e^{-\tau_{\text{B}} R_{\text{AB}}} K(\tau_{\text{B}}, \tau_{\text{A}}, R_{\text{AB}})] \tag{6}$$

where $s(\tau_{\text{A}}, R_{\text{A}})$ is a 1*s* Slater orbital centered on R_{A} with exponent τ_{A}, and $K(\tau_{\text{A}}\tau_{\text{B}}, R_{\text{AB}})$ is given by[30]

$$K(\tau_{\text{A}}, \tau_{\text{B}}, R_{\text{AB}}) = \frac{\tau_{\text{B}}^4 \tau_{\text{A}}}{2(\tau_{\text{A}}^2 - \tau_{\text{B}}^2)^2} - \frac{\tau_{\text{B}}^6 - 3\tau_{\text{B}}^4 \tau_{\text{A}}^2}{(\tau_{\text{A}}^2 - \tau_{\text{B}}^2)^3 R_{\text{AB}}} \tag{7}$$

The function γ_{AB} has the asymptotic form $(1/R_{\text{AB}})$ at long distance, and approaches γ_{AA} at the limit of $R_{\text{AB}} \to 0$.[30] The latter condition relates the decaying exponent of the spherical charge distribution to the chemical hardness (U_{A}),[43] that is

$$\tau_{\text{A}} = \frac{16}{5} U_{\text{A}} \tag{8}$$

Thus, the functional γ_{AB} is determined as soon as the chemical hardness of the atoms A and B is known.[30]

The last four terms in the second line of eq. (1) involve the reference neutral electronic density ρ_0 and E_{core}. The "repulsive potential", $E_{\text{rep}}(\rho_0)$

$$E_{\text{rep}}(\rho_0) = -\frac{1}{2} \int\int \frac{\rho_0(\vec{r}) \rho_0(\vec{r}')}{|\vec{r} - \vec{r}'|} d\vec{r} d\vec{r}' + E_{\text{xc}}[\rho_0] - \int V_{\text{xc}}[\rho_0] \rho_0(\vec{r}) d\vec{r} + E_{\text{core}} \tag{9}$$

is introduced.

With the above approximations and definitions, the total SCC-DFTB energy is given by

$$E^{\text{SCC-DFTB}} = \sum_i^{\text{occ}} \langle \phi_i | \hat{H}^0 | \phi_i \rangle + \frac{1}{2} \sum_{\text{A,B}} \gamma_{\text{AB}} \Delta q^{\text{A}} \Delta q^{\text{B}} + E_{\text{rep}} \tag{10}$$

Given the approximation eq. (5), the repulsive potential E_{rep} can be simplified. It does not depend on the charge density variation $\delta\rho$ and therefore does not contain any long-range Coulombic interactions due to the neutrality of the atomic densities. Formally, E_{rep} can be expanded in a series:

$$E_{\text{rep}}[\rho_0] = \sum_A E_{\text{rep}}[\rho_0^{\text{A}}] + \frac{1}{2} \sum_A \sum_B \{E_{\text{rep}}[\rho_0^{\text{A}} + \rho_0^{\text{B}}] - E_{\text{rep}}[\rho_0^{\text{A}}] - E_{\text{rep}}[\rho_0^{\text{B}}]\} + \cdots \tag{11}$$

The three center terms are assumed to be small and are neglected. Therefore, the repulsive potential E_{rep} is approximated as the sum of a set of pair-wise atom-atom potentials. Because ρ_0 corresponds to the charge density of a neutral atom, the electron-electron and the nucleic-nucleic repulsions cancel for large interatomic distances. Therefore, E_{rep} can be assumed to be short-ranged. However, the repulsive potential does not approach zero for large interatomic distance R_{AB}:

$$E_{\mathrm{rep}}[\rho_0] = \sum_{\mathrm{A}} E_{\mathrm{rep}}[\rho_0^{\mathrm{A}}]; \quad R_{\mathrm{AB}} \rightarrow \infty \tag{12}$$

The quantity $E_{\mathrm{rep}}[\rho_0^{\mathrm{A}}]$ contains the double-counting terms for atom A, that is, the terms in the braces in eq. (1).

Subtracting the asymptotic atomic values, we obtain the new function

$$\tilde{E}_{\mathrm{rep}}[\rho_0] = E_{\mathrm{rep}}[\rho_0] - \sum_{\mathrm{A}} E_{\mathrm{rep}}[\rho_0^{\mathrm{A}}] = \frac{1}{2} \sum_{\mathrm{A,B}} U_{\mathrm{rep}}^{\mathrm{A-B}}[\rho_0^{\mathrm{A}}, \rho_0^{\mathrm{B}}; R_{\mathrm{AB}}] \tag{13}$$

which represents the repulsive potential relative to the energy of neutral atoms; it approaches zero for large interatomic distances. The pair-wise functions $U_{\mathrm{rep}}^{\mathrm{A-B}}$ are then fitted for selected reference systems (see below) and are assumed to be transferable in calculations for more complicated molecules. It is generally important, therefore, to carry out extensive test calculations for the parameters before they are applied to a new problem.

SCC-DFTB Parameterization for Zinc

According to the above description of the SCC-DFTB approach, the required parameters for a given element include both atomic properties and interatomic repulsive potential functions. The monoatomic parameters are based on atomic DFT calculations and an optimized LCAO Slater basis set, which consists of slightly compressed atomic wave functions. Neglecting three-center integrals, the remaining two-center integrals are calculated in advance and tabulated. Therefore, the SCC-DFTB method needs no integral evaluation during its run time. The determination of the repulsive energy part is the most time consuming step in the parameterization procedure, because it is calculated as the difference of DFT and SCC-DFTB (electronic part) bond stretching energies. These repulsive energy contributions, which consist of the DFT double counting contributions, have to be determined for all pairs of atom types in the system. We describe the procedure employed to obtain these parameters for zinc in what follows.

Atomic Parameters

The required atomic properties of zinc in the SCC-DFTB framework include the LCAO basis functions χ_μ, the reference density, ρ_0, and the chemical hardness parameters, U_{A}; the last quantity determines the second order functional γ_{AB} [eq. (6) and refs. 30, 37].

The procedure to determine χ_μ is similar to that used to construct basis sets for *ab initio* or DFT methods.[44] As described above, the LCAO basis functions χ_μ are obtained from atomic Kohn-Sham calculations in the presence of the harmonic potential, $(r/r_0)^2$. The r_0 value is chosen to be 4.9 bohr for zinc, corresponding to twice the covalent radius. Calculations were performed to determine the 3d, 4s, and 4p functions with an atomic program TWOCENT; see Figure 1 for the effect of the constraining potential.

Another atomic property that needs to be determined is the reference density ρ_o, which in general is crucial for the quality of tight-binding methods.[45] In the current scheme, this is controlled by choosing the appropriate confinement potential (or the confinement radii, r_0). A weak confinement potential of radius 10.0 Å was used to damp out long-range terms, such that the resulting density is close to the atomic density.

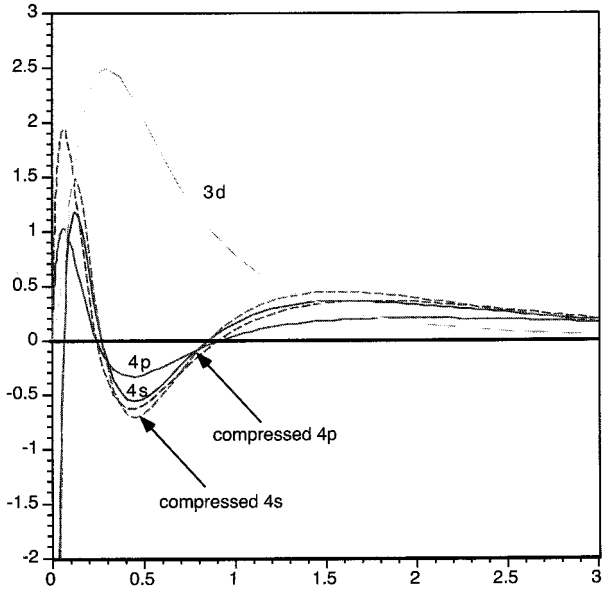

Figure 1. Atomic orbitals for zinc with (dotted) and without (soild) the harmonic constraining potentials (see text).

The chemical hardness for zinc, U_{Zn}, was calculated from an atomic DFT calculation by taking the second derivative of the total energy of an atom with respect to its total charge. The resulting value is 0.2667 hartree.

It is worth emphasizing that the atomic parameters were obtained with the charge-neutral state despite the fact that the zinc exists as a +2 ion in most proteins. This is based on the previous discussions by Slater[46] for ionic species such as NaCl. He showed that faster convergence of SCF is achieved if the initial density is based on the neutral atoms. Further, as discussed above, the choice of the charge neutral states assures that the repulsive potential is short ranged and thus more transferable.

Diatomic Parameters

After determination of the atomic parameters, the electronic part of the SCC-DFTB energy function can be readily calculated with the appropriate exchange-correlation functional; the one chosen here is the one derived by Perdew, Burke, and Ernzerhof (PBE).[47] The diatomic repulsive functions $U_{\mathrm{rep}}^{\mathrm{A-B}}$, therefore, can be determined as the following

$$U_{\mathrm{rep}}^{\mathrm{A-B}}(R_{\mathrm{AB}}) = [E_{\mathrm{tot}}(R_{\mathrm{AB}}) - E_{\mathrm{tot}}(\infty)] - \sum_i \sum_{\mu\nu} c_\mu^i c_\nu^i H_{\mu\nu}^0(R_{\mathrm{AB}}) - \frac{1}{2} \sum_{\mathrm{AB}} \gamma_{\mathrm{AB}} \Delta q^{\mathrm{A}} \Delta q^{\mathrm{B}} \tag{14}$$

where $E_{\mathrm{tot}}(R_{\mathrm{AB}}) - E_{\mathrm{tot}}(\infty)$ can be obtained from DFT calculations, and the last two terms on the right hand side (r.h.s.) can be

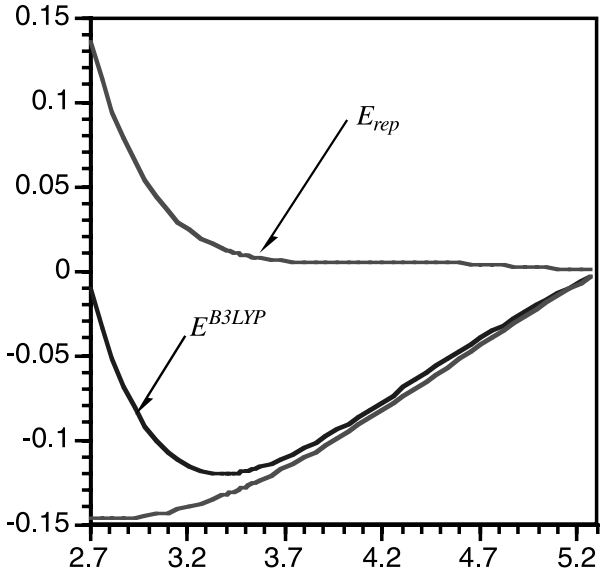

Figure 2. The quantities involved in the fitting of the Zn—N repulsive potential. The behavior is similar for other pair-wise interactions. See eq. (13) in text for details.

calculated from SCC-DFTB after the atomic parameters are determined; the atomic contributions [i.e., eq. (12)], which are constants, are ignored. This has to be done for all atomic pairs, Zn—X (X═O, N, C, H and S) at a series of interatomic distances (R_{AB}).

In principle, such a procedure can be carried out with diatomic molecules Zn—X. In practice, however, diatomic calculations often lead to SCF convergence problems due to level-crossings at larger interatomic distances. Therefore, small closed-shell molecules, where the valences of the atoms are saturated with hydrogen atoms, were used in the actual calculations to determine U_{rep}^{A-B}. For example, HZnOH was used to consider the interaction between Zn and O. Similar systems, ZnH_2, $ZnNH_2$, HZnSH, and $HZnCH_3$ were used to determine Zn—H, Zn—N, Zn—S, and Zn—C potentials, respectively. For those systems, full DFT calculations at the B3LYP[48]/6-311+G(d,p)[49] level were calculated at a series of Zn—X distances; the internal structure of other fragments (e.g., CH_3) was set to that in the equilibrium geometry of the Zn—X molecule.

As an example, results related to the Zn—N system are shown in Figure 2. It is seen that the repulsive function U_{rep}^{A-B} is short-ranged and vanishes at about 6.0 bohr. Other systems (Zn—X) exhibit very similar behaviors. It should be noted that because U_{rep}^{A-B} is limited to two-body terms here, no angular information is contained through the fitting procedure. Only information about the radial behavior of the interaction energy for the small reference systems considered is included. Therefore, the procedure is straightforward to apply, and only small reference systems have to be calculated. This contrasts to the fitting procedure in the standard semiempirical methods,[27,38] for which extensive fit to experimental data in multidimensional parameter space has to be performed. In the following section, we demonstrate that such an approach is rather effective and gives good structural and energetic properties for extensive classes of molecules containing zinc.

Test Calculations

In this section, we carry out benchmark calculations with the newly developed parameters for zinc in the SCC-DFTB framework by comparison with the results from DFT calculations (see DFT and Semiempirical PM3 Calculations). First, we examine small molecules that represent the typical coordination environment of zinc in a biological context. Properties of interest include the equilibrium geometries, ligand binding energies, and deprotonation energies of ligands bound to zinc, and dipole moments. Then, we investigate active site models for a number of zinc-containing enzymes, which include ADH, CA, and aminopeptidase. In those cases, we focus on the active site structure and energetics associated with the reactions catalyzed by the zinc ion.

DFT and Semiempirical PM3 Calculations

As a reference for the performance of the SCC-DFTB and semiempirical methods (PM3), we use the B3LYP method as implemented in GAUSSIAN98.[51] With good quality basis sets [e.g., 6-311+G(d,p) used in the current work], B3LYP has been shown to describe structures of Zn complexes in good agreement with X-ray data.[25,29] One exception is that Zn—S bond lengths are found to be overestimated by about 0.1 Å,[25d] in contrast to the local density approximation (LDA), which reproduces experimental and MP2 results surprisingly well. Despite this shortcoming, we have chosen to use the B3LYP functional because it systematically gives more reliable results for binding energies and proton affinities, which are of major importance to our work, than LDA.[50] Another shortcoming of the B3LYP method concerns the binding energy of ammonia to Zn^{2+}, which B3LYP overestimates by about 10 kcal/mol, compared to CCSD and MP2 results.[29] Therefore, in the case of NH_3 ligands, we compare binding energies with MP2/6-311+G(d,p) values. We note, however, that B3LYP and MP2 agree very well in terms of incremental ligand binding energies (see Supporting Material), which are of more importance in most applications than total binding energies of the ligands to a metal ion.

The AM1 method has been shown to be inferior to PM3 and MNDO/d for the description of Zn complexes;[29] therefore, we did not consider AM1 in this study. Both PM3 and MNDO/d (which do not include d orbitals for zinc) have shortcomings: PM3 is not reliable for the description of Zn—O bonds (also see below), especially in complexes with bulky ligands, while MNDO/d fails in the description of Zn—S bond in certain cases, and tends to exhibit large errors in the binding energy involving Zn—S interactions.[29] In the current work, we used the PM3 method as implemented in the GAUSSIAN98 program[51] for comparison with SCC-DFTB and DFT results.

Zinc–Small-Molecule Interactions

In biological systems, typical ligands for zinc ion include water, cysteine, histidine, and glutamic/aspartic acids.[2] Therefore, we have performed calculations for a series of complexes that involve the zinc ion and small molecule models for those ligands. The SCC-DFTB results were tested against B3LYP calculations with the 6-311+G(d,p) basis set for the energetics (see Supporting

Table 1. RMS Errors in SCC-DFTB and PM3 Geometry and Energetics Compared to B3LYP Calculations.[a]

Property		SCC-DFTB	PM3
Bond distances (Å)	Zn—O	0.03	0.08
	Zn—N	0.04	0.05
	Zn—S	0.04	0.05
Bond angles (°)	∠O—Zn—X	8.2	7.8
	∠N—Zn—X	3.9	3.4
	∠S—Zn—X	4.5	12.3
Total binding energy (kcal/mol)[b]	Zn—O	17.5	65.3
	Zn—N	31.0	14.3
	Zn—S	6.8	18.8
Relative binding energy (kcal/mol)[c]	Zn—O	6.8	24.6
	Zn—N	3.3	14.7
Deprotonation energy[d]	Zn—O	3.5	27.2
	Zn—S	13.3	10.1

[a]Only geometries optimized at the B3LYP/6-311 + G(d, p) level were used in the RMS error calculations.
[b]The total binding energy is defined relative to isolated zinc ion and all of its ligands. Therefore, the values are enormous (ranging from 70 to 655 kcal/mol).
[c]The relative binding energy is defined relative to the isolated unsaturated zinc-ligand complex and one ligand.
[d]Adiabatic deprotonation energies were calculated; that is, the geometries of the deprotonated species were also optimized.

Material for more details). Due to the large number of calculations required at the B3LYP level, simplified ligands were used for amino acids: H_2S or CH_3SH was used for cysteine, NH_3 or $CH_2{=}NH$ was used for histidine, and formic acid ($HCOO^-$) was used for glutamic or aspartic acids. A number of calculations were also performed with ethanol, which is the substrate of ADH. Overall, 22 species with different coordination environments for the zinc ion were studied. In addition, different protonation states for ligands such as water, cysteine, and ethanol were calculated and adiabatic deprotonation energies for those ligands were determined. They are of interest because the zinc ion catalyzes many reactions by shifting the pK_a of its bound ligand.[2] As discussed in Supporting Material, some care is required in treating the asymptotic values of the proton when calculating deprotonation energy with the SCC-DFTB method. Detailed results on the structure and energetics of those systems are given in the Supporting Material section; only the RMS errors of the SCC-DFTB results compared to B3LYP calculations are given in the main text (Table 1). For comparison, PM3 calculations were carried out, and the RMS errors compared to the B3LYP results are also given in Table 1. AM1 calculations were also performed for selected structures, and the results were consistently inferior to PM3 values and thus have not been included here. The B3LYP and PM3 calculations were made with the GAUSSIAN98 package,[51] and SCC-DFTB calculations were performed using the implementation in CHARMM.[36,37]

For the Zn—O pair, SCC-DFTB yields very reliable results, as reflected in the zinc-water/ethanol interactions in the large number of complexes considered. The RMS error in the Zn—O distance is 0.03 Å, as compared to B3LYP/6-311+G(d,p) calculations. The RMS error is 0.08 Å at the PM3 level. For instance, PM3 gives a very long Zn—O distance (3.822 Å) for ethanol binding to Zn-(His)$(Cys)_2$ (Fig. 3), while SCC-DFTB gives a value (2.288 Å) that is very close to the B3LYP result (2.198 Å). The RMS error in the bond angle ∠O—Zn—X is 8.2° and 7.8° for SCC-DFTB and PM3, respectively. The SCC-DFTB method gives improved Zn^{2+}-water/ethanol binding energies in different species compared to PM3. For the *total* ligand binding energies (i.e., binding energy of all the ligands relative to isolated species and Zn^{2+}), the RMS error is 17.5 and 65.3 kcal/mol for SCC-DFTB and PM3, respectively. Note that these absolute values are large because the total ligand binding energies are on the order of several hundred kcal/mol (the average value considered here is −243.6 kcal/mol). On a relative scale, the RMS error is 7% and 27% at the SCC-DFTB and PM3 level, respectively. The situation becomes even more favorable for SCC-DFTB if one considers the *relative* binding energy of ligands; that is, the binding energy of a water/ethanol molecule to an unsaturated zinc *complex* rather than to isolated zinc and ligand molecules. The RMS error at the SCC-DFTB and PM3 level is 6.8 and 24.6 kcal/mol, respectively. The deprotonation energies of a zinc-bound water molecule and ethanol are also well described at the SCC-DFTB level, which gives a RMS error of 3.5 kcal/mol, compared to a RMS error of 27.2 kcal/mol at the PM3 level.

Similar trends are found in the Zn—N and Zn—S interactions. The RMS errors in the Zn—N and Zn—S bond lengths are all about 0.04 Å at the SCC-DFTB level; the corresponding values are 0.05 Å for PM3. For the Zn—N distance, the SCC-DFTB calculations also agree well with X-ray structures; for example, the average Zn—N distance in a zinc-porphine complex is 2.072 Å, and the X-ray value is 2.042 Å. Note that the B3LYP/6-311+G(d,p) method was found to overestimate Zn—S bond distances in the literature by up to 0.1 Å[25a]; taking this into account, both SCC-DFTB and PM3 give satisfactory Zn—S bond lengths because both tend to give shorter values compared to B3LYP calculations (see Supporting Material). For example, compared to the X-ray structure, SCC-DFTB gives an error of 0.03 Å for the Zn—S distance in $Zn[SCH_2]_4^{2-}$, while B3LYP overestimates the bond length by 0.09 Å.[25a] The SCC-DFTB approach gives better results for the ∠S—Zn—X bond angles, and has a RMS error of 4.5°; the value at the PM3 level is 12.3°. For example, PM3 gives very different bond angles (C—S—Zn and N—Zn—S) compared to B3LYP and SCC-DFTB results for Zn(Cys)(CysH) (Fig. 3). The RMS error in the total ligand binding energy for Zn—N at the SCC-DFTB level, 31.0 kcal/mol (out of the average binding energy of −248.7 kcal/mol), is substantially larger than the PM3 value of 14.3 kcal/mol. We note, however, that B3LYP overestimates Zn-ammonia binding energies by more than 10 kcal/mol compared to MP2 and CCSD calculations.[29] Compared to MP2 total binding energies, the RMS errors in SCC-DFTB and PM3 for the Zn-ammonia complexes are 23.0 and 14.9 kcal/mol, respectively. More importantly, both SCC-DFTB and B3LYP agree well with MP2 in terms of the relative binding energies for Zn—N interactions, which are generally more important than the total binding energies of ligands on a metal ion; the RMS error is 2.3 and 2.5 kcal/mol for SCC-DFTB and B3LYP, respectively. The performance of SCC-DFTB in this regard is substantially better than PM3, which has a RMS error of 14.5 kcal/mol compared to the MP2 results. The total Zn—S binding energy is well described

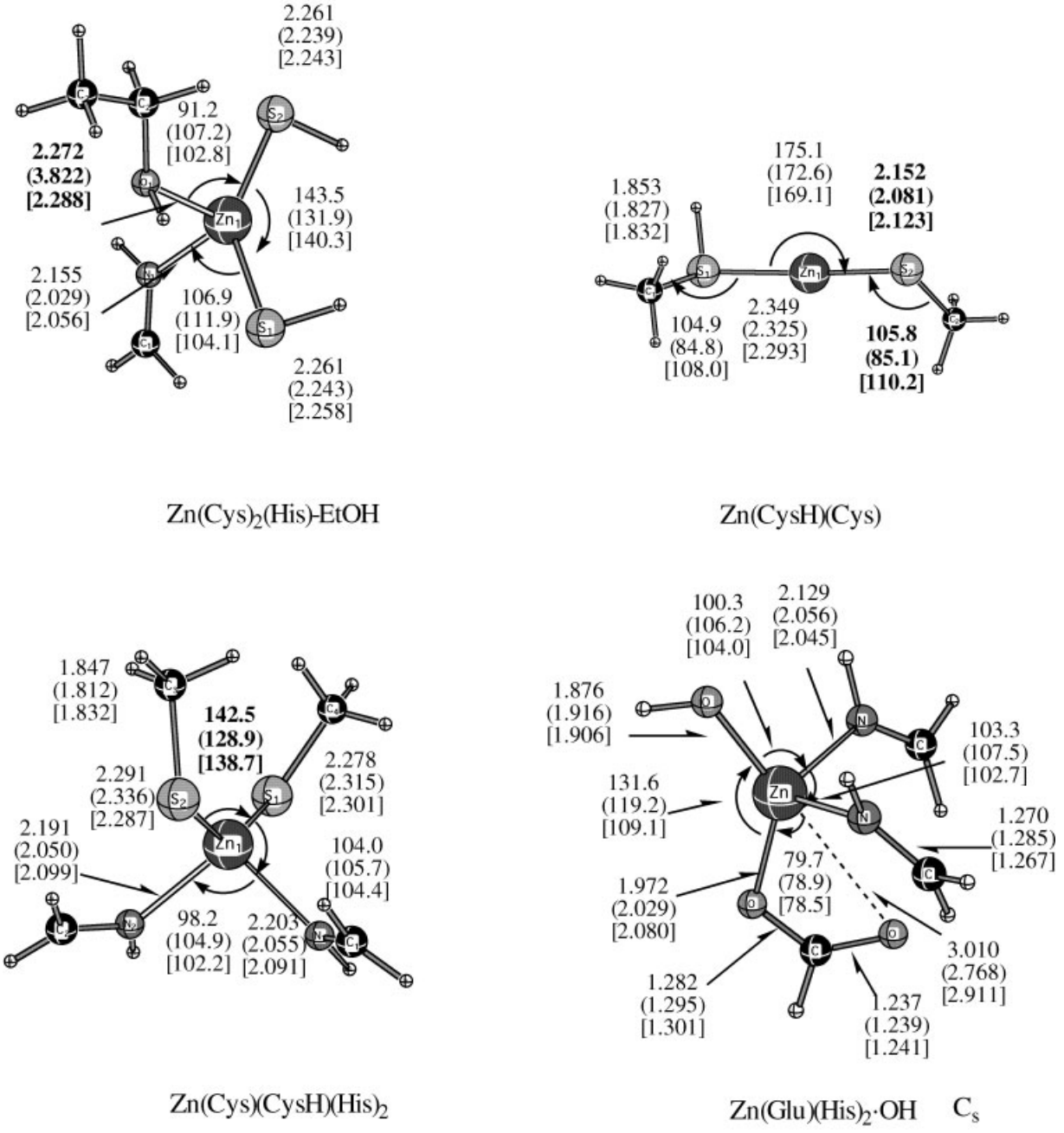

Figure 3. A few examples from the set of structures calculated to test the SCC-DFTB Zn parameters. The —SH or —SMe groups were used to mimic cystidine side chains; CH_2═NH molecule was used to model the imidazole ring in histidine; HCOO— was used to model the side chain of glutamic or aspartic acids. The numbers without parentheses were obtained at the B3LYP/6-311+G(d,p) level; those with parentheses and brackets were obtained at the PM3 and SCC-DFTB level, respectively. The bold numbers are the parameters that differ substantially at the PM3 and SCC-DFTB levels. Distances are given in angstroms and angles are given in degrees.

at the SCC-DFTB level; the RMS error is 6.8 kcal/mol (out of an average value of −423.7 kcal/mol) and 18.8 kcal/mol at the SCC-DFTB and PM3 level, respectively. The deprotonation energy of model cysteine is well described at both the SCC-DFTB and PM3 level, which has a RMS error of 13.3 and 10.1 kcal/mol, respectively.

Glutamic and aspartic acids are common ligands to zinc ions in many enzymes such as carboxypeptidase, phospholipase, and al-

kaline phosphatase.[2] As found in previous studies,[52] the coordination of Glu/Asp to zinc can be either mono- or bidentate. The energy difference between the two types of structures is usually very small, ranging from 1 to 5 kcal/mol.[52] For the system tested here (Fig. 3), both PM3 and SCC-DFTB give mono-dentate structures, while B3LYP gives bidentate coordination with a small basis set (Lanl2dz) and mono-dentate structure with a large basis set [6-311+G(d,p)]. This highlights the importance of the hydrogen-bonding interaction between the model glutamic acid and other ligands; such an interaction was also found in previous studies to be important in determining whether the mono- or the bidentate structure is more stable.[52] Both PM3 and SCC-DFTB gave satisfactory binding energies for the model glutamic acid, with a relative error of −0.08% (overestimation) and +0.02%, respectively.

Dipole moments in the SCC-DFTB method are calculated from atomic Mulliken charges. As has been pointed out earlier, they therefore give good estimates for molecular dipole moments only when they are dominated by atom-centered contributions. For various conformers of small alanine peptides, the Mullikan dipole moments were found to be in good agreement with those from B3LYP/6-31G* calculations, representing the trends between different conformers reliably, with deviations of 10% from the B3LYP values.[33] For the zinc complexes tested in the current work, both SCC-DFTB and PM3 gave reasonable values compared to B3LYP calculations. For the complexes shown in Figure 3, for example, the RMS errors in SCC-DFTB and PM3 are 0.73 and 0.95 Debye, respectively.

The above, rather extensive, tests demonstrate that the parameterization of zinc in the SCC-DFTB framework is satisfactory. Both structural and energetic results from SCC-DFTB calculations compare well to the much more expensive B3LYP calculations. Overall, the SCC-DFTB approach was found to be superior to the PM3 model, especially for the Zn—O and Zn—S interactions, which are critical in many biological systems.

Active Sits Model for Zinc-Dependent Enzymes

To further test the quality of the SCC-DFTB parameterization for the zinc ion, we studied the active site models for a number of zinc-dependent enzymes. The list includes ADH, CA, and aminopeptidase. The model calculations presented here form the basis for using the SCC-DFTB/CHARMM approach in independent studies of these enzymes.[59] As in the test calculations shown above, the SCC-DFTB results were compared to B3LYP calculations. In the B3LYP calculations, geometry optimizations were typically carried out with a double-zeta plus polarization quality basis set and an effective core potential[53] for zinc (see figure captions for details). For the single point energetics, which were used in the comparisons, the 6-311+G(d,p) basis set was used.

ADH

ADH is the enzyme that catalyzes the oxidation of alcohol to aldehyde (or further to carboxylic acid).[54] Despite numerous X-ray[7,55] and kinetic,[56] as well as theoretical, analyses,[57] important questions remain for the detailed catalytic mechanism of ADH. The proposed catalytic pathway involves a proton transfer from the zinc-bound substrate to the bulk, mediated by several active site residues (Ser48, His51) and the ribose ring in the cofactor (nicotinamide adenine dinucleotide, NAD^+), and a hydride transfer from the substrate to the NAD^+. Recent theoretical analyses suggest that the proton transfers precede the hydride transfer, and that the former proceeds in a step-wise fashion. As to the hydride transfer, much attention has been paid to the effect of hydride tunneling and possible promoting vibrational modes in the enzyme.[58] Interesting kinetic experiments related to those issues exist, although convincing explanations for the observations are not yet available. Detailed theoretical analysis might provide useful insights that complement the experimental approach. Because both the issues of chemical reaction (hydride transfer) and enzyme dynamics have to be taken into consideration in such studies, an efficient QM/MM approach such as SCC-DFTB/CHARMM is ideal. Here we study the hydride transfer in ADH using a simple model and demonstrate the capability of the SCC-DFTB approach with the newly developed parameters for zinc. A detailed study on the proton and hydride transfer in the presence of the enzyme environment using the SCC-DFTB/CHARMM approach has been published separately.[59]

As shown in Figure 4, the SCC-DFTB approach gives rather reliable geometries for not only the stable structures, but also the saddle point. The hydride-donor and hydride-acceptor distance is 1.202 and 1.501 Å, respectively, at the SCC-DFTB level; the corresponding values are 1.232 and 1.507 Å with the B3LYP approach associated with the double-zeta plus polarization function quality basis set. The nature of the transition state, therefore, is rather early at both levels. This is consistent with the fact that the reaction is exothermic, by 8.8 and 5.2 kcal/mol at the SCC-DFTB and B3LYP single point with the 6-311+G(d,p) basis set, respectively. The barrier height is 7.9 and 8.2 kcal/mol at the two levels, respectively (see also Appendix). The PM3 approach was found to be unreliable for the current system and gave severely distorted structures. Therefore, only single point energy calculations at the B3LYP optimized structures are reported. The PM3 approach significantly overestimates the exothermicity of the reaction and gives a value of −46.7 kcal/mol. In addition, it gives a *lower* energy at the saddle point relative to the reactant by 3.2 kcal/mol.

CA

CA is the enzyme that catalyzes the interconversion of CO_2 and HCO_3^- (bicarbonate).[60] The alpha class CAs are zinc-containing monomeric proteins with a molecular mass around 30 KDa, and are involved in a number of physiological processes such as respiration and formation of secretory fluids.[61] Experimental[60,62] and theoretical[10,63] analyses suggest that the reaction proceeds in two stages. In the hydration direction, the first stage involves a proton transfer from the zinc-bound water molecule to the bulk through a histidine residue (H64) and presumably a number of active site water molecules. This generates a zinc-bound hydroxyl ion, which then reacts with the CO_2 and forms the product bicarbonate. The mechanism has been generally accepted, although certain issues such as the kinetics of the substrate binding/dissociation,[64] the detailed proton transfer[65] dynamics, and kinetic isotope effects are still under investigation. Here we use the SCC-DFTB method to study models for the two types of reactions

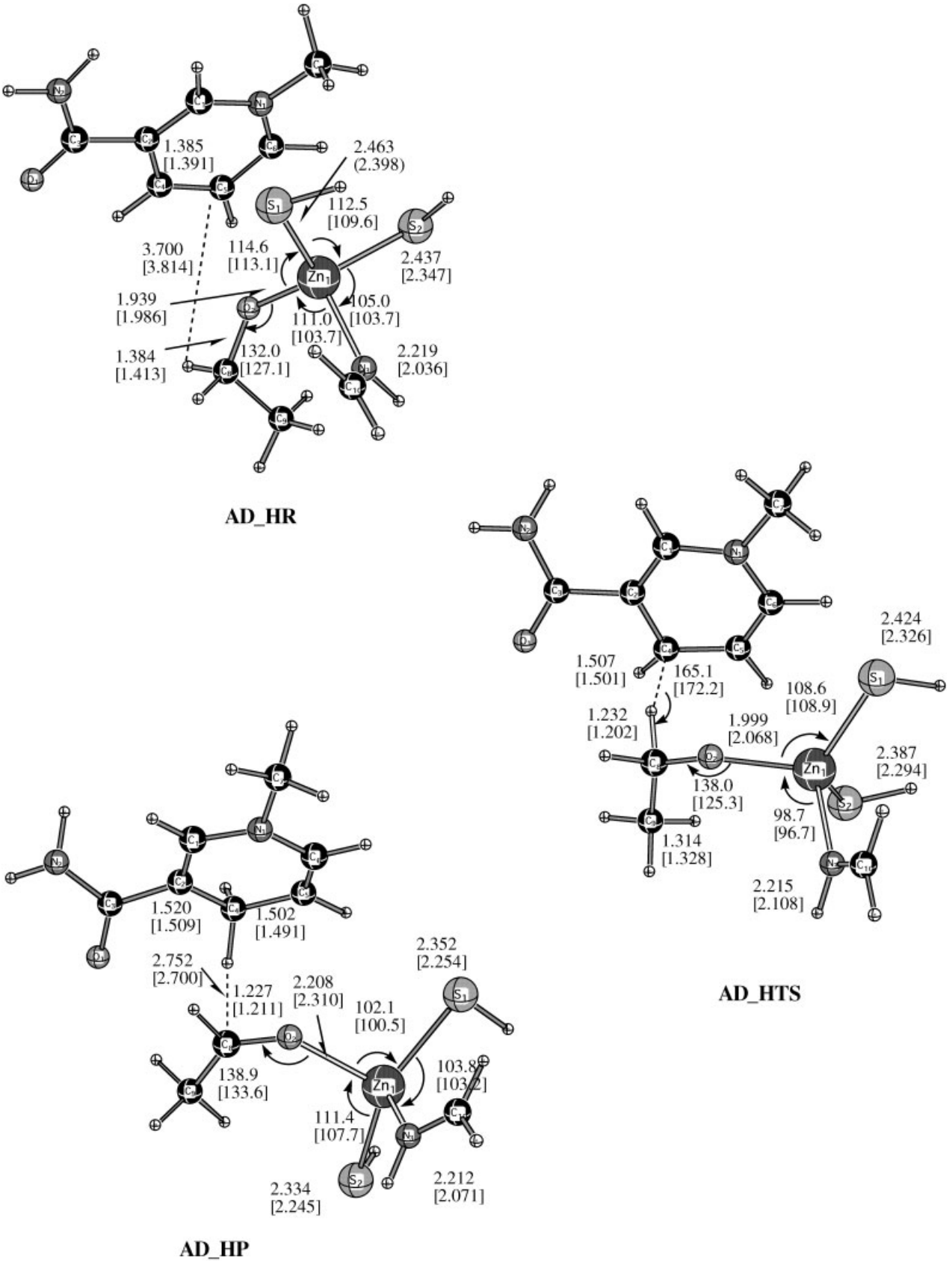

Figure 4. Optimized model structures involved in the hydride transfer in the liver alcohol dehydrogenase. Distances are given in angstroms and angles are in degrees. The numbers without parentheses or brackets were obtained at the B3LYP level with double-zeta plus polarization quality basis set: Lanl2dz for Zn; Lanl2dz augmented with polarization d function for S; and 6-31G(d) for the others. The values in the parentheses are single point PM3 values at the B3LYP optimized geometries (see text); those in the brackets were obtained with the SCC-DFTB method.

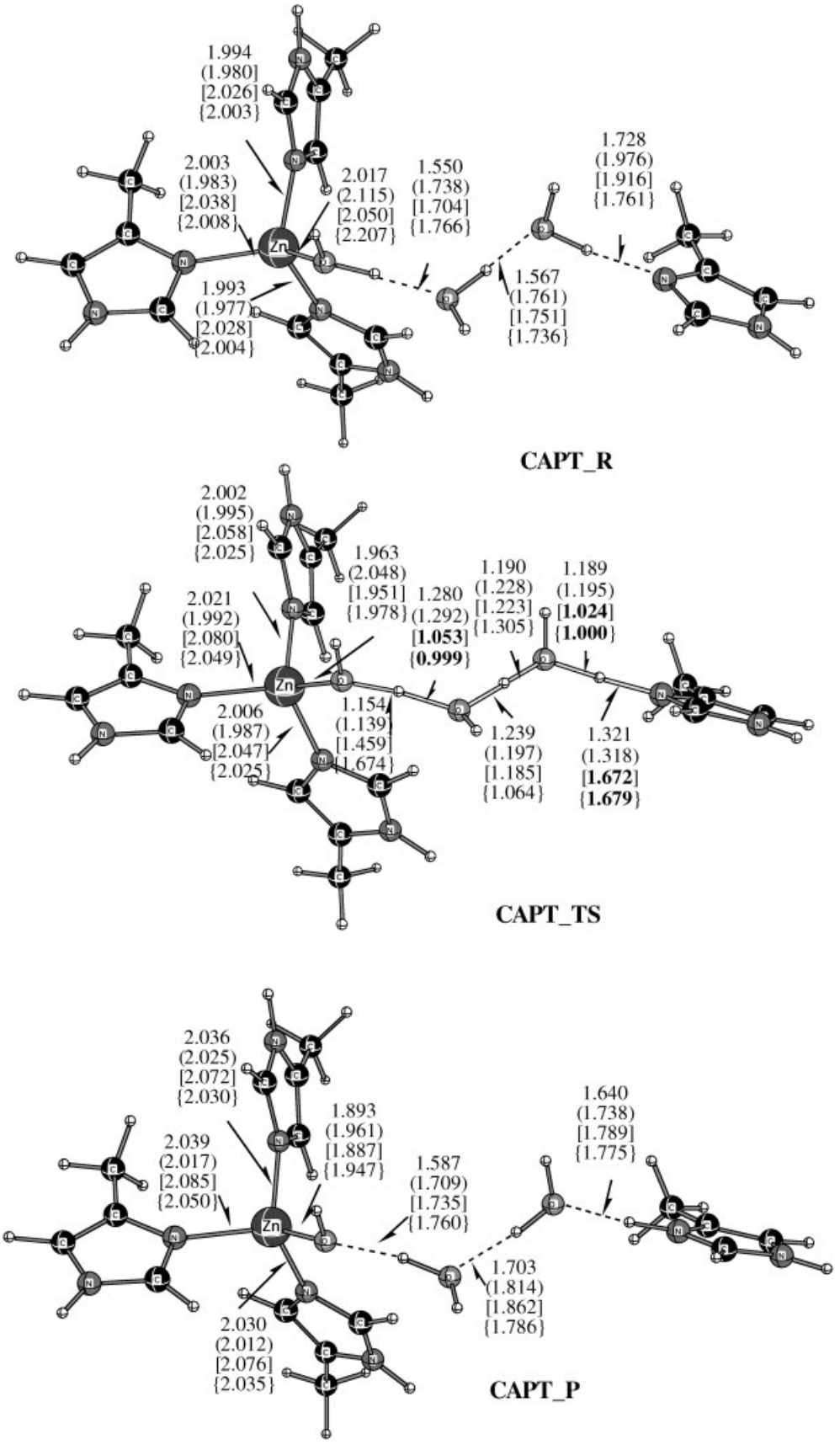
1.994
(1.980]
[2.026]
{2.003}
2.003
(1.983)
[2.038]
{2.008}
2.017
(2.115)
[2.050]
{2.207}
1.550
(1.738)
[1.704]
{1.766}
1.728
(1.976)
[1.916]
{1.761}
1.567
(1.761)
[1.751]
{1.736}
1.993
(1.977)
[2.028]
{2.004}
Zn
CAPT_R
2.002
(1.995)
[2.058]
{2.025}
1.963
(2.048)
[1.951]
{1.978}
1.190
(1.228)
[1.223]
{1.305}
1.189
(1.195)
[1.024]
{1.000}
2.021
(1.992)
[2.080]
{2.049}
1.280
(1.292)
[1.053]
{0.999}
2.006
(1.987)
[2.047]
{2.025}
1.154
(1.139)
[1.459]
{1.674}
1.239
(1.197)
[1.185]
{1.064}
1.321
(1.318)
[1.672]
{1.679}
Zn
CAPT_TS
2.036
(2.025)
[2.072]
{2.030}
1.893
(1.961)
[1.887]
{1.947}
1.640
(1.738)
[1.789]
{1.775}
2.039
(2.017)
[2.085]
{2.050}
1.587
(1.709)
[1.735]
{1.760}
1.703
(1.814)
[1.862]
{1.786}
2.030
(2.012)
[2.076]
{2.035}
Zn
CAPT_P

Figure 5.

and to illustrate the advantages and limitations of the SCC-DFTB approach.

Intramolecular Proton Transfer CA has been used as a prototype to illustrate the mechanism of proton transfer reactions in enzyme. Two types of proton transfer reactions were found to be relevant. The intramolecular proton transfer involves the zinc-bound water molecule and a histidine residue on the surface of the protein (H64 in CA-II); the intermolecular proton transfer occurs between the histidine residue and the bulk solvent. Solvent kinetic isotope effects suggest that the intramolecular proton transfer is rate limiting in well-buffered solution.[62] The kinetics of the intramolecular proton transfer have been well studied and interpreted in the framework of Marcus theory extended to proton transfer reactions.[65a,66] It was found that the experimental data can be fitted into the Marcus theory only if a large work term (about 10 kcal/mol) is invoked. The origin of this work term is not clear, although it has been suggested to involve either orienting the water bridges in the active site or a flip of the His 64 side chain from an outward to inward orientation.[65a] It has also been suggested that an additional intermediate state has to be included. This leads to a three-state Marcus model,[67] which can fit the experimental data without the large work term.[65a,67] The energetics associated with the proton transfers in CA have been analyzed theoretically by a number of authors[65b,67,68]; only the recent work of Voth and coworkers[65b] makes use of a fairly high level of quantum mechanical theory. It was found[65b] that water molecules can assist proton transfer between a model histidine (or a zinc-bound water) and a water molecule by stabilizing the product and thereby lowering the activation barrier. The donor-acceptor distance was found to be critical in determining the barrier height, as has been realized by many authors.[69] The ligand of the zinc was also found to be important in determining the barrier height for proton transfer involving the zinc-bound water.[65b] The possible role of a hydrogen bonded water chain in the proton transfer in CA is well accepted; the detailed character of the pathway, however, is not clear from these studies. For example, no transition state searches were performed in ref. 65b, and therefore it is not clear whether the proton transfer, which is assisted by the water chain, is step-wise or concerted and if there is a hydronium intermediate.[67] Here we carry out model calculations for a scenario with one bridging water to illustrate the SCC-DFTB approach, and leave the results with more bridging water molecules to a separate publication.[70]

As shown in Figure 5, the proton transfer is highly *concerted* at both the B3LYP and SCC-DFTB level, and the transferring proton is equally shared between the donor and acceptor atoms. The agreement between the SCC-DFTB and B3LYP geometries is made more encouraging by noting that both PM3 and Hartree-Fock gave rather different transition state structures. At the saddle point from PM3 and HF, the first proton transfer (from the zinc-bound water to the free water) is nearly completed while the second proton transfer (from the free water to histidine) has yet to occur. The energetics at the SCC-DFTB level are in semiquantitative agreement with the B3LYP results. The barrier is 8.1 and 5.9 kcal/mol at the SCC-DFTB and B3LYP level, respectively; the exothermicity of the reaction is −0.8 (i.e., endothermic) and +4.9 kcal/mol at the two levels, respectively. Both PM3 and HF overestimate the barrier significantly and give values around 20 kcal/mol.

The approximate agreement between SCC-DFTB and B3LYP is very encouraging and opens up the possibility of studying the detailed mechanism and rates for the proton transfer in CA. The effect of the quantum mechanical nature of the proton can also be addressed using either semiclassical models or by path-integral techniques. Such calculations are in progress.[70]

Interconversion of CO_2 and Bicarbonate The mechanism of the interconversion of CO_2 and bicarbonate has been studied theoretically by a number of authors.[10,63] Here we restrict ourselves to the few structures considered in previous studies.[63,71] Similar to ref. 71, we used NH_3 to model the histidine in the active site.

As shown in Figure 6, the SCC-DFTB gives a reasonable, though not exact, description for the weak complex (Com1) between CO_2 and $Zn^{2+}(NH_3)_3$ moiety. The distance between the oxygen in CO_2 and Zn is 2.911 and 3.128 Å at the SCC-DFTB and B3LYP level, respectively. The binding energy is well described by the SCC-DFTB approach; it is 7.1 kcal/mol compared to the value of 5.3 kcal/mol at the B3LYP level. Interestingly, CO_2 does not bind to the zinc at the PM3 level.

The exothermicity of the reaction is substantially underestimated at both the SCC-DFTB and PM3 level, compared to the B3LYP calculations. The product complex Com2 is −4.0 kcal/mol compared to isolated CO_2 and $Zn^{2+}(NH_3)_3$ at the B3LYP level; SCC-DFTB and PM3 give a value of +5.0 and +0.9 kcal/mol, respectively. As a result, the barrier is substantially higher at the latter two levels, 14.1 and 19.1 kcal/mol, respectively, compared to the value of 3.1 kcal/mol at the B3LYP level. The structure of the saddle point at the SCC-DFTB and PM3 levels is also substantially later than that at the B3LYP level, in accord with the Hammond postulate. For example, the forming oxygen-carbon bond is 1.931, 1.697, and 1.544 Å at the B3LYP, PM3, and SCC-DFTB level, respectively. As described in the section DFT and Semiempirical PM3 Calculations, SCC-DFTB gives a good description of the Zn—O interaction; therefore, the poor results obtained here appear to be due to the description of the C═O double bond breaking (into a single bond in the current reaction). Indeed, this is a rather difficult quantity for DFT, in general, especially if exact exchange is not used (which is the case for SCC-DFTB). The difficulty is illustrated by the fact that the CO_2 atomization energy is substantially overestimated at the PBE level compared to B3LYP calculations.[72]

Figure 5. (*continued*) Optimized structures of species involved in the model proton transfer reaction in carbonyl anhydrase. The Cβ atoms for the histidine residues were obtained from the X-ray structure (ref. 78) and were fixed in the geometry optimizations. Distances are given in angstroms and angles are in degrees. The values without parentheses or brackets were obtained at the B3LYP level with the 6-31G(d) basis set for all the atoms (including Zn). The numbers with parentheses were obtained at the SCC-DFTB level; those with square brackets and braces were obtained at the PM3 and HF/6-31G(d) level, respectively.

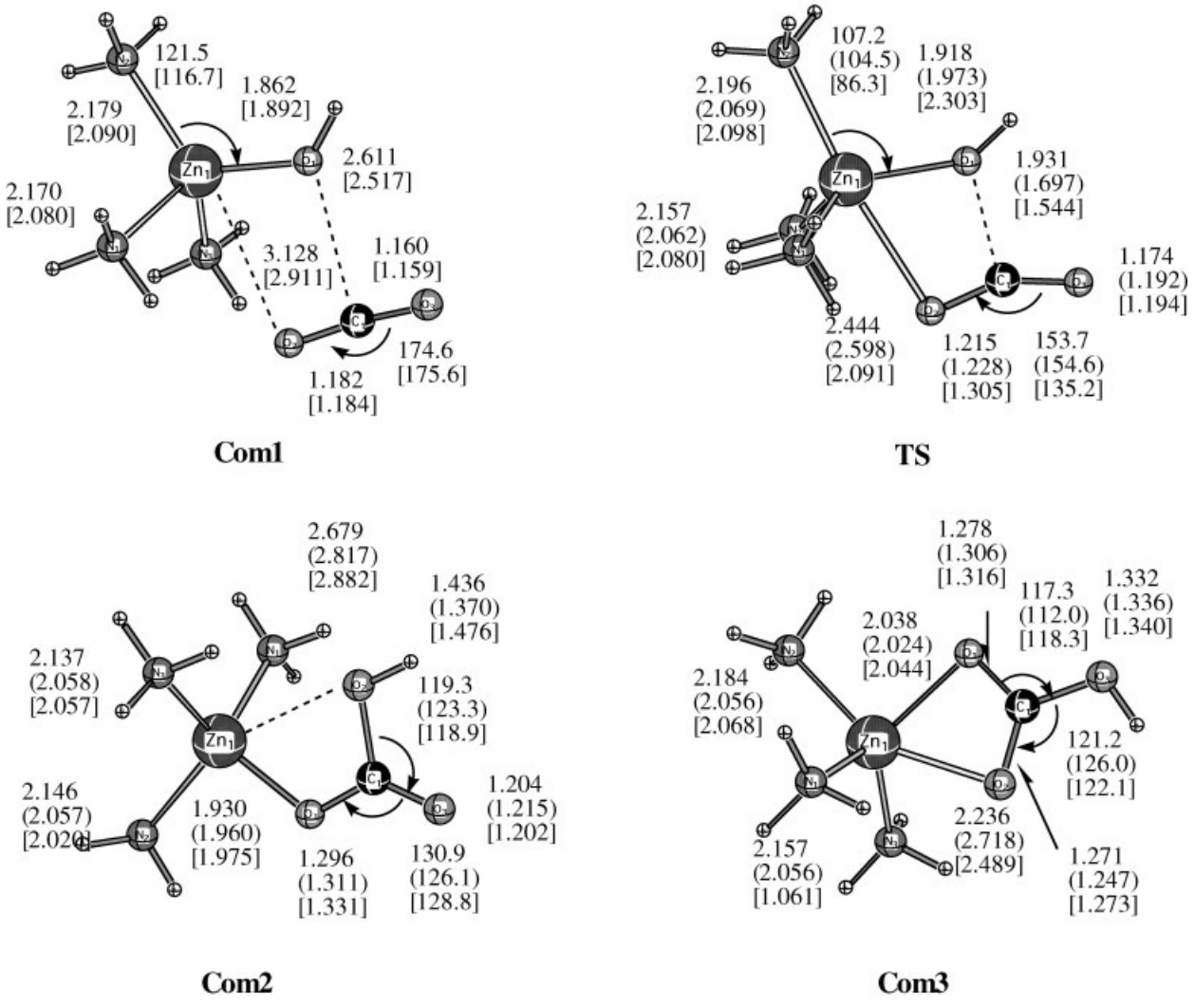

Figure 6. Optimized structures of species involved in the model hydration reaction in carbonyl anhydrase. Distances are given in angstroms and angles are in degrees. The numbers without parentheses or brackets were obtained at the B3LYP level with double-zeta plus polarization quality basis set (see Fig. 3 caption); those in the parentheses are PM3 values; those in the brackets were obtained with the SCC-DFTB method.

As described in early studies, there is another binding conformation for the bicarbonate to the zinc, which is shown as Com3 in Figure 6. Similar to the situation for glutamic acid binding discussed above, both PM3 and SCC-DFTB predicted a mono-dentate structure while B3LYP gives a nearly bidentate binding conformation. The relative energy of Com2 and Com3, however, is well described at both PM3 and SCC-DFTB levels; the values are 7.4 and 7.7 kcal/mol, respectively, compared to the value of 6.2 kcal/mol at the B3LYP level.

Summarizing, the examples for CA demonstrate that SCC-DFTB is a promising approach for describing reactions involving zinc ion. However, it also has limitations originating from the fact that an approximate exchange functional was used and therefore may give poor descriptions in cases where nonhybrid DFT methods have problems.

Di-Nuclear Zinc Site of Aminopeptidase

A large number of enzymes require metal cofactors for either catalytic or structural reasons. A smaller, but continuously growing fraction, of those contain well-defined constellations of metal ions in their active sites, which has been shown to be essential for catalysis.[73] One of these is the "bridged binuclear metal" motif. In its general form it consists of two metal cations (usually divalent, such as zinc) bridged by an endogenous ligand (usually a Glu or Asp carboxylate, coordinating the metals in a bidentate fashion), an exogenous one (a water molecule, a substrate, a hydroxide), or both. These metallohydrolases perform phosphate ester, as well as peptide bond, hydrolysis. They are involved in processes including DNA repair, hormone regulation, tissue repair, protein maturation, and carcinogenesis.[74] The relatively simple, small, and symmetric

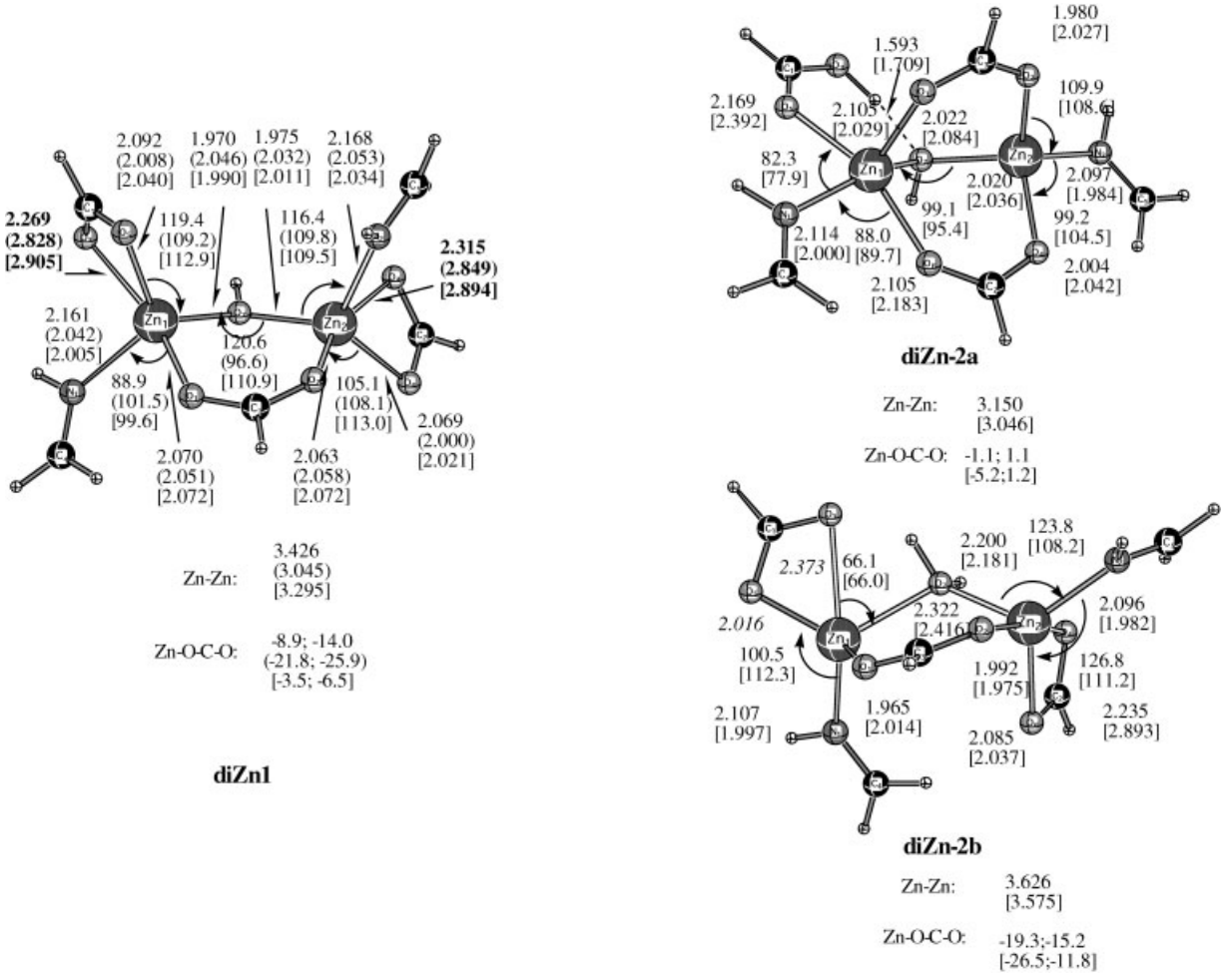

Figure 7. Optimized structures of di-nuclear Zn^{2+} complexes with carboxylic ligands. Distances are given in angstroms and angles are in degrees. The numbers without parentheses or brackets were obtained at the B3LYP level with double-zeta plus polarization quality basis set (see Fig. 3); those in the parentheses are PM3 values; those in the brackets were obtained with the SCC-DFTB method. In diZN2b, the distances in italics are kept frozen during geometry optimizations to prevent proton transfer from the bridging water molecule to the carboxylic group.

active site of *Aeromonas Proteolytica* Aminopeptidase (AAP)[75] is a prime candidate for mechanistic studies of binuclear metallopeptidases. This is especially true because crystal structures of AAP-inhibitor complexes are available at high resolution.[76] There remain questions regarding the role of the metals in the AAP mechanism, as well as of the identity of the nucleophile. It is also of interest that AAP is 80% active with one Zn only, while in the case of bovine lens leucine aminopeptidase (blLAP),[77] which has a similar active site and catalyzes the same reaction, both metals are required. Clearly, it is important to determine if the AAP mechanism is the same or similar with one or two metals in the active site.

As shown in Figure 7, both PM3 and SCC-DFTB give a stable structure for the di-Zn species when the bridging water is ionized (i.e., an OH^- ion). The overall structures at those levels are very similar to that from the B3LYP calculation, except for the binding mode of model glutamic acids, as also seen in the previous section. The PM3 approach gives a much shorter Zn—Zn distance and therefore a sharper Zn—O(H)—Zn angle (see Fig. 7). The orientation of the bridging glutamic acid at the SCC-DFTB level is closer (see the dihedral angles shown in Fig. 7) to the B3LYP results than that of the PM3 calculation. The binding energy of the bridging OH^- is calculated to be 223.3 kcal/mol at the PM3 level, which is very close to the value of 222.2 kcal/mol from B3LYP calculations; the SCC-DFTB approach gives a somewhat larger value of 236.9 kcal/mol (Table 2).

When the bridge is a water molecule, one of its protons is transferred to a model glutamic acid ligand. As a result, another glutamic acid also becomes bridged between the two zinc ions leading to three bridging ligands (two glutamic acid plus one OH^-); this leads to diZn-2a (Fig. 7). Such a rearrangement is not expected within an enzyme active site, where each of the

Table 2. Energetics in kcal/mol for the Active Site Model for Several Enzymes (Alcohol Dehydrogenase, Carbonic Anhydrase, and Aminopeptidase).[a]

Enzyme	Species	B3LYP	SCC-DFTB	PM3
LADH[a]	AD_R			
	AD_TS	8.2	7.9	(−3.2)[c]
	AD_P	−5.2	−8.8	(−46.7)[c]
CA	CAPT_R			
Proton	CAPT_TS	5.9	8.1	23.7
Transfer[b]	CAPT_P	−4.9	+0.8	−8.2
	$Zn(NH_3)_3(OH)^- + CO_2$			
	Com1	−5.3	−7.1	—[d]
Hydration[a]	TS	3.1	14.1	19.1
	Com2	−4.0	5.0	0.9
	Com3	−10.2	−2.7	−6.5
AP[a]	Di—Zn · OH^-[e]	−222.2	−236.9	−223.3
	Di—Zn · H_2O[e]	−31.9 [−307.9]	−29.3 [−317.5]	— [—]

[a]The structures were optimized at the B3LYP level with the following basis sets: Lanl2dz for Zn; Lanl2dz augmented with *d* polarization function for S; and 6-31G(d) for the others. Single point energies were calculated with the 6-311 + G(d,p) basis set. For the structures involved in liver alcohol dehydrogenase (LADH), proton transfer in carbonic anhydrase (CA), CO_2 hydration in CA, and aminopeptidase (AP), see Figs. 4, 5, 6, and 7, respectively. For LADH and proton transfer in CA, the energetics are relative to the reactant complexes (AD_R and CAPT_R, respectively); for CO_2 hydration in CA, the energy reference is isolated $Zn(NH_3)_3(OH^-)$ and CO_2. For AP, see footnote e.

[b]The 6-31G(d) basis set was used for all the atoms, including the zinc atom.

[c]The PM3 structures were not stable; single point energy calculations were performed at the B3LYP optimized structures.

[d]The CO_2 dissociated during geometry optimization at the PM3 level.

[e]For these complexes, the value without parentheses is the binding energy of H_2O to diZN-2b, and the number with brackets is the binding energy of OH^- to diZN-2a (see text and Fig. 7).

ligands is constrained by the protein backbone and is involved in interactions with other side chains and/or water molecules. Therefore, the O—Zn distances of the carboxylate interacting with the bridging water molecule are frozen and a partial optimization is restarted from a plateau on the potential energy surface just before the rearrangement occurs; this leads to diZn-2b. In both cases, PM3 leads to dissociation of the carboxylate ligands. The SCC-DFTB approach, by contrast, gives structures that are similar to the B3LYP calculations. The binding energy (Table 2) of the bridging water (OH^-) in diZn-2b (diZn-2a) is also well described at the SCC-DFTB level, which is 29.3 (317.5) kcal/mol, compared to the value of 31.9 (307.9) kcal/mol from B3LYP calculations.

Conclusions

Zinc ion has many important functions in biological systems. An efficient and accurate quantum mechanical description for zinc is crucial for the use of theoretical methods to study the multiple roles of the zinc ion. In the current work, a parameterization for zinc has been developed in the framework of the SCC-DFTB. The SCC-DFTB method was chosen based on its already demonstrated success in describing structural and energetic properties for species involving main group elements.[30,35]

The parameterization was tested with a range of systems, which includes small molecules that contain the typical coordination environment of zinc (with cysteine, histidine, and glutamic/aspartic acids and water), and active site models for a number of zinc-containing enzymes, such as ADH, CA, and aminopeptidase. Properties such as geometries, total and relative ligand binding energies, deprotonation energies of ligands, as well as barriers for the reactions in active site models of enzymes were studied. The SCC-DFTB results were compared with B3LYP calculations with triple-zeta plus polarization functions quality basis sets for the energetics; comparison was also made with the standard PM3 method. The SCC-DFTB approach showed substantial improvements over the PM3 method in many aspects, particularly in the binding energies and deprotonation energies of ligands that bind through the oxygen atom (e.g., water and ethanol). The SCC-DFTB method also gave better structural and energetic properties compared to PM3 for proton transfer reactions aided by the zinc ion, as in the model of CA. In the case of aminopeptidase, the structural integrity of the di-zinc site was maintained well at the SCC-DFTB level, while PM3 was not able to give stable structures.

The current parameterization of zinc for SCC-DFTB is quite accurate and transferable. Because the parameterization method is relatively straightforward, it can be extended to other metal ions such as copper and iron, though they are expected to be more

complicated because of their open-shell character. This opens up the exciting possibility of exploring the catalytic mechanisms of metalloenzymes in more detail than has been possible in the past, and of considering dynamical features that are critical in the enzyme function, such as proton pumping in cytochrome c oxidase.

Supporting Materials

Detailed structures and energetics for model complexes at different levels (B3LYP and SCC-DFTB) are included as supporting materials.

Appendix I. Calculations of Proton Affinity

As mentioned in the main text [eq. (13)], the total energy in the DFTB method is defined with respect to the atomic contributions $E_{\mathrm{rep}}[\rho_0^{\mathrm{A}}]$. For reactions between neutral compounds, this shift can be neglected because it occurs on both sides of the reaction equation. In the case of deprotonation reactions, however, we have to consider these terms explicitly.

To calculate energies of the reaction

$$BH^+ \rightarrow B + H^+$$

with the DFTB method, the energy of the proton according to eq. (10) has to be considered:

$$E(H^+) \;=\; 0.5 * U_{\mathrm{H}} \;=\; -131.6\ \mathrm{kcal/mol}$$

In case of the H atom, $E_{\mathrm{rep}}[\rho_0^{\mathrm{A}}]$ equals the self-interaction energy and is equal to $0.5*U_{\mathrm{H}}$.

We can also calculate $E_{\mathrm{rep}}[\rho_0^{\mathrm{H}}]$ using eq. (13), that is

$$E_{\mathrm{rep}}[\rho_0^{\mathrm{H}}] = E^{\mathrm{DFT}} - E_{\mathrm{elec}}^{\mathrm{DFTB}} = [E_{\mathrm{tot}}^{\mathrm{DFT}}(R_{\mathrm{AB}}) - E_{\mathrm{tot}}^{\mathrm{DFT}}(\infty)] - \sum_i \sum_{\mu\nu} c_\mu^i c_\nu^i H_{\mu\nu}^0(R_{\mathrm{AB}}) - \frac{1}{2}\sum_{\mathrm{AB}} \gamma_{\mathrm{AB}} \Delta q^{\mathrm{A}} \Delta q^{\mathrm{B}}$$

where E^{DFT} is the energy of the H-atom at the DFT level, which is -0.4977 hartree at the BLYP/6-31++G** level of theory (i.e., *not* free of self-interaction). $E_{\mathrm{elec}}^{\mathrm{DFTB}}$ is the electronic energy contribution of the SCC-DFTB model [first two terms in eq. (9)] and equals -0.27160 hartree. With these values, we find $E_{\mathrm{rep}}[\rho_0^{\mathrm{H}}]$ is equal to -141.8 kcal/mole, which differs by about 10 kcal/mol from $0.5*U_{\mathrm{H}}$.

In other words, to be fully consistent, one should set U_{H} to be $2*\ E_{\mathrm{rep}}[\rho_0^{\mathrm{H}}]$; in practice, however, it is calculated numerically as the derivative of the HOMO energy with respect to the occupation number, where only small variations around the neutral atom are considered.[30] Although this scheme works well for larger ions, where only a small portion of the total electronic charge is removed from or added to the system, it does not reproduce the ionization potential well in the case of H^+, where the total charge is removed from the system. Here, the perturbational approach, which relies on the second-order expansion of the DFTB energy with respect to charge variations, becomes inexact.

To calculate deprotonation energies, we evaluate the energy difference of the protonated and deprotonated complex and have to correct for the missing self-interaction of the H-atom due to eq. (11). In an earlier publication,[37] we calculated proton affinities using the value -131.6 kcal/mole for $E_{\mathrm{rep}}[\rho_0^{\mathrm{H}}]$. However, this value is not the correct self-interaction energy and in this work, we used the value of 141.8 kcal/mol. For the study of proton transfer reactions, however, the choice of the value -131.6 or -141.8 kcal/mol does not make any difference, because the contribution cancels out for the relative energies.

References

1. See, for example: (a) Girard, C.; Kagan, H. B. Angew Chim Intl Ed 1998, 37, 2922; (b) Darensbourg, D. J.; Holtcamp, M. W. Coord Chem Rev 1996, 153, 155; (c) Knochel, P.; Singer, R. Chem Rev 1993, 93, 2117.
2. For recent reviews, see for example: (a) Lipscomb, W. N.; Sträter, N. Chem Rev 1996, 96, 2375; (b) Christianson, D. W.; Cox, J. D. Ann Rev Biochem 1999, 68, 33; (c) Vallee, B. L.; Auld, D. S. Acc Chem Res 1993, 26, 543; (d) Vallee, B. L.; Auld, D. S. Biochem 1993, 32, 6493.
3. See for example: (a) Chapman Jr, W. H.; Breslow, R. J Am Chem Soc 1995, 117, 5462; (b) Molenveld, P.; Kapsabelis, S.; Engbersen, H. F. J.; Reinhoudt, D. N. J Am Chem Soc 1997, 119, 2948.
4. Christianson, D. W. Adv Prot Chem 1991, 42, 281.
5. See, for example: Berg, J. M. Ann Rev Biophys Biophys Chem 1990, 19, 405.
6. Klug, A.; Schwabe, J. W. R. FASEB J 1995, 9, 597; (b) Berg, J. M.; Shi, Y. Science 1996, 271, 1081.
7. Eklund, H.; Palpp, B. V.; Samama, J. P.; Brändén, J. J Biol Chem 1982, 257, 14359.
8. Honzatko, R. B.; Crawford, J. L.; Monaco, H. L.; Ladner, J. E.; Edwards, B. F. P.; Evans, D. R.; Warren, S. G.; Wiley, D. C.; Ladner, R. C.; Lipscomb, W. N. J Mol Biol 1982, 160, 219.
9. (a) Coleman, J. E. Annu Rev Biochem 1992, 61, 897; (b) Vallee, B. L.; Coleman, J. E.; Auld, D. S. Proc Natl Acad Sci USA 1991, 88, 999; (c) Christianson, D. W. Adv Protein Chem 1991, 42, 281.
10. (a) Liang, J.; Lipscomb, W. N. Biochem 1987, 26, 5293; (b) Liang, J.; Lipscomb, W. N. Biochem 1988, 27, 8676.
11. (a) Christianson, D. W.; Lipscomb, W. N. Acc Chem Res 1989, 22, 62; (b) Lipscomb, W. N. Proc Natl Acad Sci USA 1980, 77, 3875.
12. Estévez, A. G.; Crow, J P.; Sampson, J. B.; Reiter, C.; Zhuang, Y. X.; Richardson, G. J.; Tarpey, M. M.; Barbeito, L.; Beckman, J. S. Science 1999, 286, 2498.
13. Hough, E.; Hansen, L. K.; Birknes, K.; Jynge, K.; Hansen, S.; Horvik, A.; Little, C.; Dodson, E.; Derewenda, Z. Nature 1989, 338, 357.
14. Kim, E. E.; Wyckoff, H. W. J Mol Biol 1991, 218, 449.
15. Maret, W.; Larsen, K. S.; Vallee, B. L. Proc Natl Acad Sci USA 1997, 94, 2233.
16. (a) Vendani, A.; Huhta, D. W. J Am Chem Soc 1990, 112, 4759; (b) Hoops, S. C.; Anderson, K. W.; Merz Jr, K. M. J Am Chem Soc 1991, 113, 8262.
17. Ryde, U. Proteins 1995, 21, 40.
18. (a) Makinen, M. W.; Troyer, J. N.; van der Werff, H.; Berendsen, J. C.; van Gunsteren, W. F. J Mol Biol 1989, 207, 210; (b) Liang, J.; Lipscomb, W. N. Proc Natl Acad Sci USA 1990, 87, 3675.
19. Stote, R. H.; Karplus, M. Proteins 1995, 23, 12.
20. Stote, R. H.; Karplus, M. To appear.

21. See, for example: (a) Gresh, N.; Claverie, P.; Pullman, A. Int J Quant Chem 1986, 29, 101; (b) Gresh, N. J Phys Chem 1997, 101, 8680.
22. Tiraboschi, G.; Roques, B-P.; Gresh, N. J Comput Chem 1999, 20, 1379.
23. See, for example: (a) Gresh, N. J Comput Chem 1995, 16, 8556; (b) Gresh, N.; Garmer, D. R. J Comput Chem 1996, 17, 1581; (c) Bock, C. W.; Kaufman-Katz, A.; Markham, G. D.; Glusker, J. P. J Am Chem Soc 1999, 121, 7360.
24. (a) Hartmann, M.; Clark, T.; Van Eldik, R. J Am Chem Soc 1997, 119, 7843; (b) Pavlov, M.; Seigbahn, P. E. M.; Sandstorem, M. J Phys Chem A 1998, 102, 219.
25. (a) Tirabischi, G.; Gresh, N.; Giessner-Prettre, C.; Perdersen, L. G.; Deerfield, D. W. J Comput Chem 2000, 21, 1011; (b) Deerfield, D. W.; Carter Jr, W. C.; Pedersen, L. G. Int J Quantum Chem 2001, 83, 150; (c) Cheng, F. et al. J Phys Chem B 2002, 106, 4552; (d) Dudev, T.; Lim, C. J Phys Chem B 2001, 105, 10709.
26. Dewar, M. J. S.; Zoebisch, E. G.; Healy, E.; Stewart, J. J. P. J Am Chem Soc 1985, 107, 3902.
27. Stewart, J. J. P. J Comput Chem 1989, 10, 209.
28. Thiel, W.; Voityuk, A. A. J Phys Chem 1996, 100, 616.
29. Bräuer, M. et al. J Mol Struct THEOCHEM 2000, 505, 289.
30. Elstner, M.; Porezag, D.; Jungnickel, G.; Elsner, J.; Haugk, M.; Frauenheim, T.; Suhai, S.; Seifert, G. Phys Rev B 1998, 58, 7260.
31. Goringe, C. M.; Bowler, D. R.; Hernandez, E. Rep Prog Phys 1997, 60, 1447.
32. Elstner, M.; Porezag, D.; Jungnickel, G.; Frauenheim, T.; Suhai, S.; Seifert, G. MRS Symp Proc 1998, 491, 131.
33. (a) Bohr, H. G.; Jalkanen, K. J.; Elstner, M.; Frimand, K.; Suhai, S. Chem Phys 1999, 246, 13; (b) Elstner, M.; Jalkanen, K. J.; Knapp-Mohammady, M.; Frauenheim, T.; Suhai, S. Chem Phys 2000, 256, 15; (c) Elstner, M.; Jalkanen, K. J.; Knapp-Mohammady, M.; Frauenheim, T.; Suhai, S. Chem Phys 2001, 263, 203.
34. (a) Ditchfield, R.; Hehre, W. J.; Pople, J. A. J Chem Phys 1971, 54, 724; (b) Hehre, W. J.; Ditchfield, R.; Pople, J. A. J Chem Phys 1972, 56, 2257; (c) Hariharan, P. C.; Pople, J. A. Theor Chim Acta 1973, 28, 213.
35. (a) Elstner, M.; Porezag, D.; Frauenheim, Th.; Suhai, S.; Seifert, G. MRS Symp Proc; Pittsburgh, PA, 1999; (b) Elstner, M.; Frauenheim, T.; Kaxiras, E.; Seifert, G.; Suhai, S. Phys Stat Sol B 2000, 217, 357.
36. Brooks, B. R.; Burccoleri, R. E.; Olafson, B. D.; States, D. J.; Swaminathan, S.; Karplus, M. J Comp Chem 1983, 4, 187.
37. (a) Cui, Q.; Elstner, M.; Kaxiras, E.; Frauenheim, T.; Karplus, M. J Phys Chem B 2001, 105, 569; (b) Han, W.; Elstner, M.; Jalkanen, K. J.; Frauenheim, T.; Suhai, S. Int J Quantum Chem 2000, 78, 459.
38. Dewar, M. J. S.; Thiel, W. J Am Chem Soc 1977, 99, 4899.
39. Porezag, D.; Frauenheim, T.; Köhler, T.; Seifert, G.; Kaschner, R. Phys Rev B 1995, 51, 12947.
40. Eschrig, H. Optimized LCAO Methods and the Electronic Structure of Extended Systems; Akademie Verlag: Berlin, 1998; p 1.
41. Handbook of Chemistry and Physics, 78th Ed.; CRC Press: New York, 1997.
42. Pariser, R. J Chem Phys 1956, 24, 250.
43. Parr, R. G.; Pearson, R. G. J Am Chem Soc 1983, 105, 7512.
44. See, for example: Dunning Jr, T. H.; Hay, P. J. In Methods of Electronic Structure Theory; Shaefer III, H. F., Ed.; Plenum Press: New York, 1977; p 1.
45. Foulkes, W.; Haydock, R. Phys Rev B 1989, 39, 12520.
46. Slater, J. C. Quantum theory of molecules and solids, Vol. 4, The self-consistent field for molecules and solids; McGraw-Hill: New York, 1994.
47. Perdew, J. P.; Burke, K.; Ernzerhof, M. Phys Rev Lett 1996, 77, 3865.
48. (a) Becke, A. D. Phys Rev A 1998, 38, 3098; (b) Lee, C.; Yang, W.; Parr, R. G. Phys Rev B 1988, 37, 785; (c) Becke, A. D. J Chem Phys 1993, 98, 5648.
49. (a) Krishnan, R.; Binkley, J. S.; Seeger, R.; Pople, J. A. J Chem Phys 1980, 72, 650; (b) Hariharan, P. C.; Pople, J. A. Theor Chim Acta 1973, 28, 213; (c) Clark, T.; Chandrasekhar, J.; Spitznagel, G. W.; von R. Schleyer, P. J Comput Chem 1983, 4, 294.
50. See, for example: Koch, W.; Holthausen, M. C. A chemist's guide to density functional theory; Wiley: New York, 2001; p 1.
51. Frisch, M. J.; Trucks, G. W.; Schlegel, H. B.; Scuseria, G. E.; Robb, M. A.; Cheeseman, J. R.; Zakrzewski, V. G.; Montgomery, J. A. J.; Stratmann, R. E.; Burant, J. C.; Dapprich, S.; Millam, J. M.; Daniels, A. D.; Kudin, K. N.; Strain, M. C.; Farkas, O.; Tomasi, J.; Barone, V.; Cossi, M.; Cammi, R.; Mennucci, B.; Pomelli, C.; Adamo, C.; Clifford, S.; Ochterski, J.; Petersson, G. A.; Ayala, P. Y.; Cui, Q.; Morokuma, K.; Malick, D. K.; Rabuck, A. D.; Raghavachari, K.; Foresman, J. B.; Cioslowski, J.; Ortiz, J. V.; Stefanov, B. B.; Liu, G.; Liashenko, A.; Piskorz, P.; Komaromi, I.; Gomperts, R.; Martin, R. L.; Fox, D. J.; Keith, T.; Al-Laham, M. A.; Peng, C. Y.; Nanayakkara, A.; Gonzalez, C.; Challacombe, M.; Gill, P. M. W.; Johnson, B.; Chen, W.; Wong, M. W.; Andres, J. L.; Gonzalez, C.; Head-Gordon, M.; Replogle, E. S.; Pople, J. A. GAUSSIAN98, Revision A.6; Gaussian, Inc.: Pittsburgh, PA, 1998.
52. Ryde, U. Biophys J 1999, 77, 2777.
53. (a) Hay, P. J.; Wadt, W. R. J Chem Phys 1985, 82, 270; (b) Hay, P. J.; Wadt, W. R. J Chem Phys 1985, 82, 284; (c) Hay, P. J.; Wadt, W. R. J Chem Phys 1985, 82, 299.
54. (a) Klinman, J. P. Crit Rev Biochem 1981, 10, 39; (b) Pettersson, G. Crit Rev Biochem 1987, 21, 349.
55. Ramaswamy, S.; Eklund, H.; Plapp, B. V. Biochem 1994, 33, 5230.
56. (a) Shearer, G. L.; Kim, K.; Lee, K. M.; Wang, C. K.; Plapp, B. V. Biochem 1993, 32, 11186; (b) Ramaswamy, S.; Park, D. H.; Plapp, B. V. Biochem 1999, 38, 13951.
57. Agarwal, P. K.; Webb, S. P.; Hammes-Schiffer, S. J Am Chem Soc 2000, 122, 4803.
58. (a) Bahnson, B. J.; Park, D. H.; Kim, K.; Plapp, B. V.; Klinman, J. P. Biochem 1993, 32, 5503; (b) Bahnson, B. J.; Colby, T. D.; Chin, K. J.; Goldstein, B. M.; Klinman, J. P. Proc Natl Acad Sci USA 1997, 94, 12797.
59. Cui, Q.; Elstner, M.; Karplus, M. J Phys Chem B 2002, 106, 2721.
60. See, for example: (a) Silverman, D. N.; Vincent, S. H. CRC Crit Rev Biochem 1983, 14, 207; (b) Silverman, D. N.; Lindskog, S. Acc Chem Res 1988, 21, 30.
61. Dodgson, S. J.; Tashian, R. E.; Gross, G.; Carter, N. D. The Carbonic Anhydrases; Plenum Press: New York, 1991.
62. (a) Steiner, H.; Jonsson, B. –H.; Lindskog, S. Eur J Biochem 1975, 59, 253; (b) Simonsson, I.; Jonsson, B. –H.; Lindskog, S. Eur J Biochem 1979, 93, 409; (c) Silverman, D. N.; Tu, C. K.; Lindskog, S.; Wynns, G. C. J Am Chem Soc 1979, 101, 6734.
63. See, for example: (a) Zheng, Y.; Merz Jr, K. M. J Am Chem Soc 1992, 114, 10498; (b) Jacob, O.; Cardenas, R.; Tapia, O. J Am Chem Soc 1990, 112, 8692; (c) Toba, S.; Colombo, G.; Merz Jr, K. M. J Am Chem Soc 1999, 121, 2290.
64. Merz Jr, K. M.; Banci, L. J Am Chem Soc 1997, 119, 863.
65. See, for example: (a) Silverman, D. N. Biochimica et Biophysica Acta 2000, 1458, 88; (b) Lu, D.; Voth, G. J Am Chem Soc 1998, 120, 4006.
66. Silverman, D. N.; Tu, C. K.; Chen, X.; Tanhouser, S. M.; Kresge, A. J.; Laipis, P. J Biochem 1993, 32, 10757.
67. Warshel, A.; Hwang, J. K.; Åqvist, J. Faraday Discuss 1992, 93, 225.
68. (a) Liang, J.; Lipscomb, W. N. J Am Chem Soc 1986, 108, 5051; (b) Merz Jr, K. M.; Hoffmann, R; Dewar, M. J. S. J Am Chem Soc 1989, 111, 5636; (c) Zheng, Y.; Merz Jr, K. M. J Am Chem Soc 1992, 114, 10498.
69. For an interesting discussion, see for example: Borgis, D.; Hynes, J. T.

In The enzyme catalysis process; Cooper, A., Houben, J. L., Chien, L. C., Eds.; Plenum Press: New York, 1988.
70. Cui, Q.; Karplus, M., to be published.
71. Stanton, R. V.; Merz Jr, K. M. J Chem Phys 1994, 100, 434.
72. Zhang, Y.; Yang, W. Phys Rev Lett 1998, 80, 890.
73. (a) Wilcox, D. Chem Rev 1996, 96, 2435; (b) Dismukes, G. C. Chem Rev 1996, 96, 2909; (c) Holm, R. H. et al. Chem Rev 1996, 96, 2239.
74. (a) Pelletier, H.; Sawaya, M. R.; Kumar, A.; Wilson, S. H.; Kraut, J. Science 1994, 264, 1891; (b) Volbeda, A.; Lahm, A.; Sakiyama, F.; Suck, D. EMBO 1991, 10, 1607; (c) Stŕter, N.; Klabunde, T.; Tucker, P.; Witzel, H.; Krebs, B. Science 1995, 268, 1489; (d) Stamper, C.; Bennett, B.; Holz, R. C.; Ringe, D.; Petsko, G. A. Biochem 2001, 40, 7035.
75. (a) Chevrier, B., et al. Structure 1994, 2, 283; (b) Chevrier, B., et al. FEBS 1996, 237, 393; (c) DePaola, C. C., et al. Biochemistry 1999, 9048, 38.
76. Desmarais, W. T. Personal communication.
77. (a) Sträter, N.; Lipscomb, W. N. Biochemistry 1995, 34, 9200; (b) Sträter, N.; Lipscomb, W. N. Biochemistry 1995, 34, 14792.
78. Hakansson, K.; Carlsson, M.; Soensson, L. A.; Liljas, A. J Mol Biol 1992, 227, 1192.